17th World Conference on Earthquake Engineering, 17WCEE
Sendai, Japan - September 27th to October 2nd, 2021

BOND FAILURE OF RC BEAMS WITH INDUCED CORROSION CRACKS BY ALUMINUM PIPE FILLED WITH AN EXPANSION AGENT

A. S. Syll [(1)], T. Aburano [(2)], K. Fujiwara T[(3)]. Kanakubo [(4)]

[(1)] *Graduate School of Systems and Information Engineering, University of Tsukuba, s2030203@s.tsukuba.ac.jp*
[(2)]*Graduate School of Systems and Information Engineering, University of Tsukuba, s1920881@s.tsukuba.ac.jp*
[(3)] *Graduate School of Systems and Information Engineering, University of Tsukuba, s2020869@s.tsukuba.ac.jp*
[(4)]*Division of Engineering Mechanics and Energy, University of Tsukuba, Ph.D, kanakubo@kz.tsukuba.ac.jp*

Abstract

Rebar corrosion is the most observed deterioration mechanism in reinforced concrete (RC) structures. When located in seismic zones, this damage over time may have adverse effects on their seismic performance. Therefore, it is necessary to evaluate the effect of degradation on the seismic performance of RC structures. In order to study the problem, experimental tests on damaged beam specimens have been conducted under anti-symmetrical bending loads.

Monitoring surface crack width is a popular tool for assessing the service life of RC structures. Surface crack provides the most apparent visual manifestation of corrosion. In this study, the simulation of the cracking of concrete due to corrosion of reinforcing bars by using an expansion agent filled pipe (EAFP) is adopted. One advantage of this method is that it allows focusing on the more fundamental effect of the cracking while ignoring the section loss of corroded rebar. After the cracking simulation, one of the four RC beam specimens was transversally cut to observe the internal cracking situation. Further, the three beam specimens with three different levels of crack width were loaded.

The specimen with larger induced crack width failed by bond degradation along the induced cracks. However, comparative analysis of the results showed that the correlation between maximum shear capacity of specimens and induced crack width was not clear enough. Therefore, the degradation of loading capacity due to induced crack cannot be merely evaluated with the crack width parameter. The significant modifications of service behavior were observed, due to the bond degradations, namely: loss of initial stiffness and reduction of accumulated energy absorption.

Keywords: bar corrosion; surface crack width; bond behavior; expansion agent; anti-symmetrical bending load

1. Introduction

It is urgent to address the safety problems caused by corrosion of reinforcing bars (rebars) in structural concrete members. This phenomenon has been recognized to be one of the most significant causes of deterioration for reinforced concrete (RC) structures. The corrosion products expand the volume of corroded steel reinforcement, leading to tensile stresses that can cause the cover concrete cracking of these RC structures. Also, when located in seismic zones, this damage over time may have adverse effects on the seismic performance of these constructions. Studies over the past two decades have provided important information on the deterioration of these members. It has previously been observed that the shear capacity is affected by corrosion of reinforcement. The previous studies conclusively reported the degradation of shear capacity and ductility of RC [1,2]. But, other studies have drawn attention to the fact that the shear capacity is increased by the loss of bond due to corrosion-induced cracking along longitudinal reinforcement [3].

The accelerated corrosion techniques have been adopted in several studies on the performance degradation of cracked concrete RC structures. In these techniques, it can be challenging to control the widths or patterns of the cracks. Also, the combination of concrete cracking and sectional defect of the rebar leads to difficulties in analyzing the degradation process at a fundamental level. On another hand, Murai et al. [4] studied the performance of RC beams with simulated cracks due to corrosion. The cracks were formed by inserting thin slits (e.g., propylene sheet). While the use of slits to simulate cracking is easy to implement, the conformity to real cracks remains unclear. In this study, the simulation of the cracking of concrete due to corrosion of reinforcing bars by using an expansion agent filled pipe (EAFP) [5,6] is adopted. One advantage of this method is that it allows focusing on the effect of the cracking while ignoring the section loss of corroded rebar.

This study aims to contribute to this growing area of research by exploring the effect of bond deterioration on the shear capacity of deteriorated RC beams. To achieve this goal, first, different damage level (crack width) is simulated to the specimens by inducing cracks using an EAFP. Finally, to grasp the mechanical performance of the damaged beam, anti-symmetrical loading test of the damaged beam are carried out.

2. Experimental program

2.1 Test specimens

The specimens are listed in Table 1, and the arrangement of the reinforcement is shown in Fig.1. In the four RC specimens fabricated in this study, the damage was simulated with three different levels (target crack width). To observe the condition of internal cracking simulation, one of them with level 3 damage is transversally cut (Monitor specimen). Then, the three others were subjected to an anti-symmetrical loading. The cross-section of the specimen is 220 mm x 420 mm with a target central region of 1260mm and a shear span of 1.5. Four D16 deformed rebars in two layers and D10@200 deformed rebars were used as a stirrup. To simulate the cracking damage, four aluminum pipes with an outer diameter of 22mm and thickness of 1mm were used as EAFP.

As seen in Table 2, RC beam specimens were structurally designed to have higher shear capacities than flexural and bond ones. The flexural, shear and bond capacities of the specimen are calculated by formulas for sound RC members by the Architectural Institute of Japan [7,8].

Table 1 – List of specimens

Specimen ID	Commons factors	Damage: Maximum induced crack width
Level.1	Target central region: 1260mm Shear span ratio: 1.5 Stirrup ratio: 0.32%	$\omega_{cr} \leqq 0.2$mm
Level.2		$0.2 < \omega_{cr} \leqq 0.8$mm
Level.3		$0.8\text{mm} < \omega_{cr}$
Monitor		$0.8\text{mm} < \omega_{cr}$

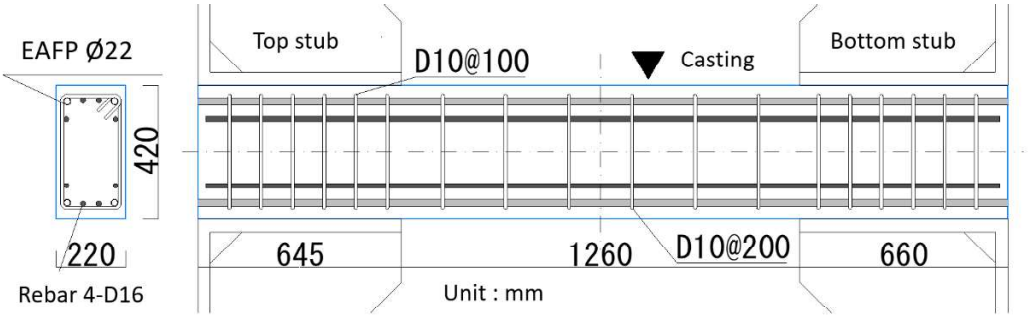

Fig.1 – Arrangement of bar

Table 2 – Calculation of capacities

Flexural capacity Q_{Mu} (kN)	Shear capacity V_u (kN)	Bond capacity V_{bu} (kN)	Shear margin index V_u / Q_{Mu}	Bond margin index V_{bu} / Q_{Mu}
204	180	251	0.88	1.23

2.2 Used materials

The concrete, provided by a local ready-mixed concrete factory, was made with an ordinary Portland cement with a content of 248 kg/m^3, a water-cement ratio of 78.5%, and maximum aggregate grain size of 20 mm. The concrete mix details are given in Table 3. The mechanical characteristics of the concrete measured at loading day on ϕ100mm×200mm cylinder are summarized in Table 4. The main bar is D16 and the stirrup is D10. SD490 was used for D16, and SD295 was used for D10. Tensile test results of reinforcing bars are listed in Table 5. An aluminum pipe with an outer diameter of 22mm and thickness of 1mm was used as EAFP. Tensile test results of the aluminum pipe are listed in Table 6.

Table 3 – Concrete mix details

Water-cement ratio (%)	Cement (kg/m^3)	Water (kg/m^3)	Fine Aggregate (kg/m^3)	Coarse Aggregate (kg/m^3)	Water reducing agent (kg/m^3)
78.5	248	195	930	840	2.48

Table 4 – Mechanical characteristics of concrete

Target strength	Compressive strength (MPa)	Elastic modulus (GPa)	Splitting strength (MPa)
18 MPa	20.5	18.2	2.07

Table 5– Mechanical characteristics of reinforcing bar

Type	Yield strength (MPa)	Tensile strength (MPa)	Elastic modulus (GPa)	Elongation at rupture (%)
D16	526	703	192	14.8
D10	352	481	190	30.4

Table 6 – Mechanical characteristics of aluminum pipe

Offset strength (MPa)	Tensile strength (MPa)	Elastic modulus (GPa)	Poisson's ratio
207	235	60	0.338

2.3 Anti-symmetrically loading and measurement method

Fig.2. illustrates the loading test setup. The specimens were vertically raised. The rotation of the top stub of a specimen was restricted by two vertical jacks and results in the anti-symmetric moment distribution of the central beam test region. In this system vertical movement of the top stub was free, that is, no additional vertical load was applied to the specimen. Lateral shear force was applied by a horizontal 100 tons actuator. During the test, the drift angle of the specimen was controlled. Shear force, the relative displacement between stubs, the axial displacement between stubs, the strain of main bars, stirrups, and aluminum pipes were measured. The drift angle is obtained from relative displacement between stubs divided by clear span length. The loading history is shown in Fig.3.

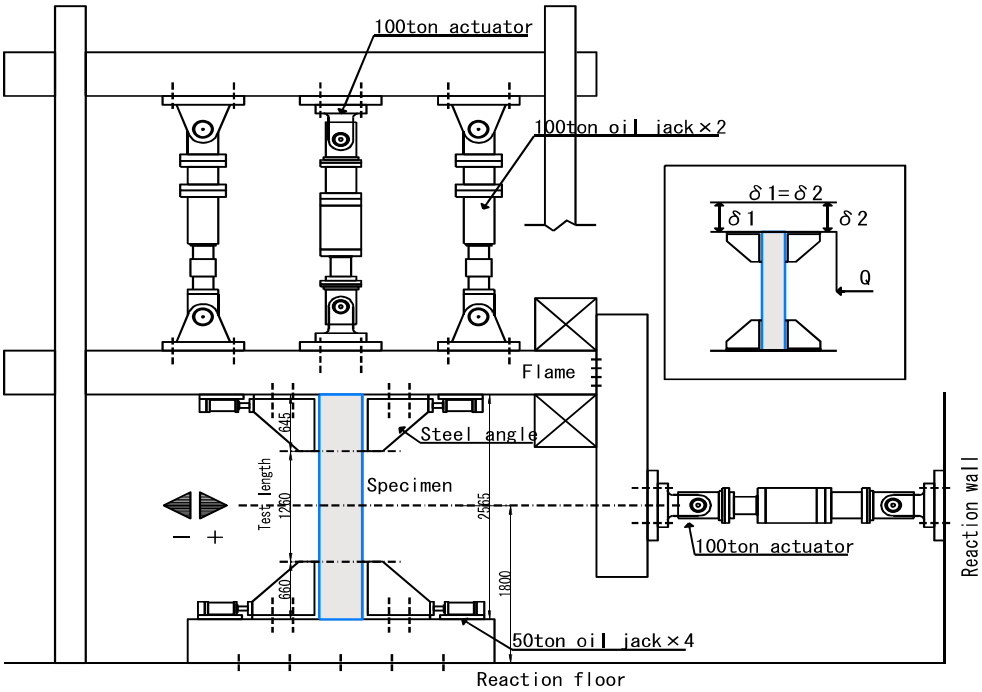

Fig.2 – Loading system

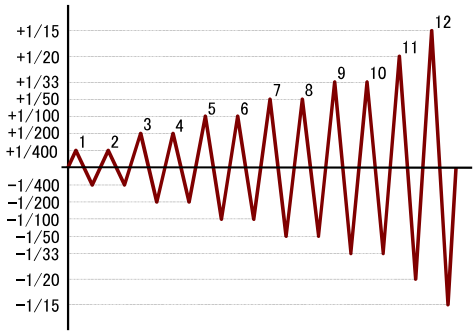

Fig.3 – Loading history

3. Experimental results

3.1 Visual assessment of induced crack by EAFP

To simulate the cracking due to volumetrically expansion of rebars, the RC beam was vertically raised, and an expansion agent mixed with 30% of water was filled into the aluminum pipes. Hours after filling, longitudinal

cracks running parallel to the reinforcing bars were measured and recorded as shown in Fig. 4. The value in the figure indicates the maximum crack widths measured in each section. Focusing on the casting direction, it can be observed that cracks width at the top is smaller than those at the bottom of the beam. It seems possible that these results are due to the change of the EAFP expansion transmission due to the presence of voids during the cure of the concrete.

Besides, to observe the internal cracking condition, three transversal cuts were performed on a beam with level 3 damage. The detail of internal cracking can be seen in Fig.5. The value in the figure expresses the surface crack width. It can be seen that the distribution of cracks was non-uniform along the axis of the beam. Also, side split cracks mostly occurred around the first layer due to the expansion of EAFP. In some cases, cracks progressed till the main bar of the second layer.

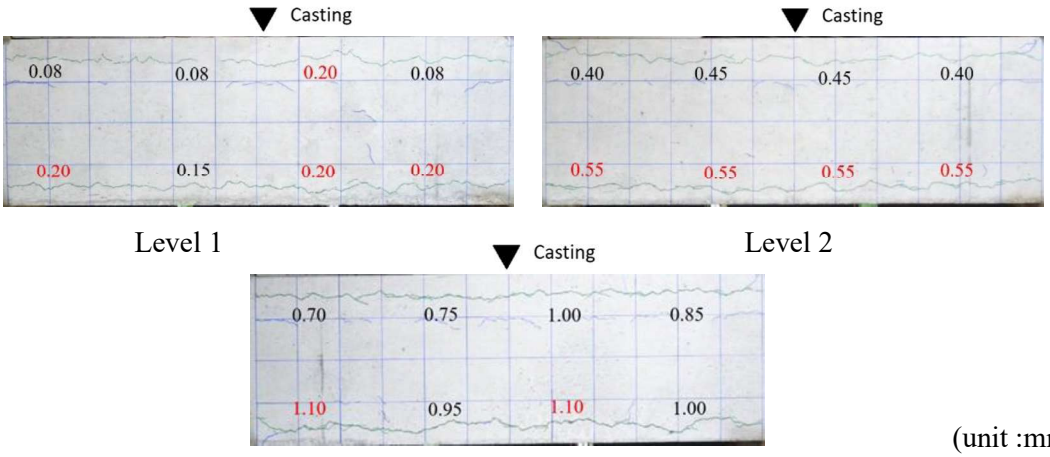

(unit :mm)

Fig.4 – Crack simulated by EAFP before loading

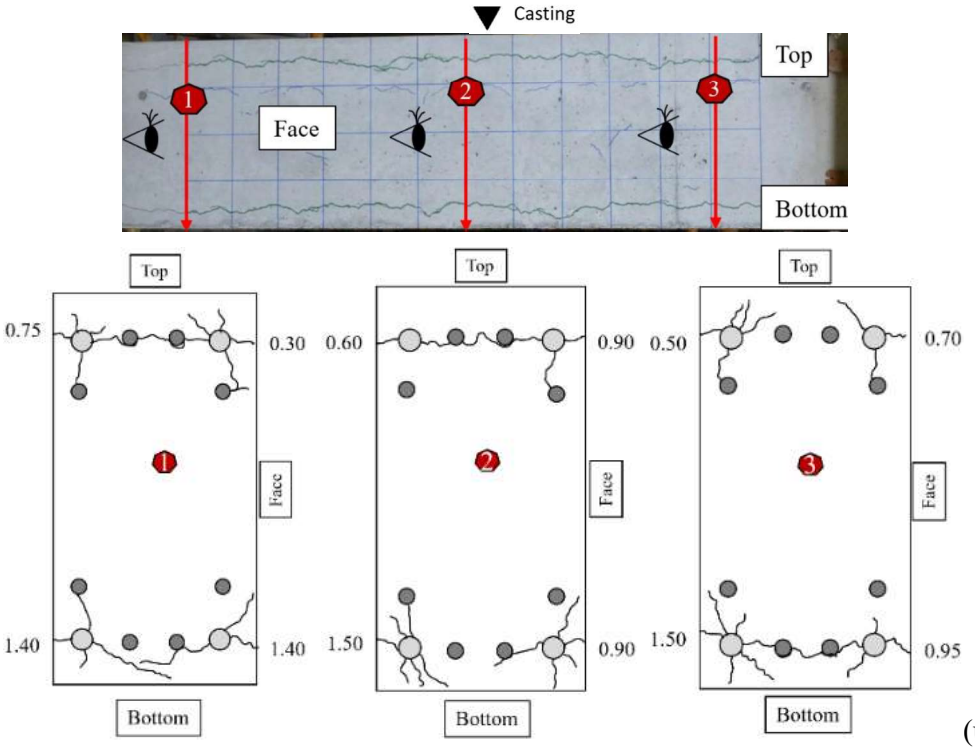

(unit :mm)

Fig.5 – Detail of internal cracking

3.2 Failure pattern

Fig. 6 shows the crack patterns of the damaged specimen at 1/100 rad and 1/50 rad as drift angle, where the induced cracks by EAFP before the anti-symmetrical loading are marked in green color. During the loading, cracks that occurred at positive loading are in blue and in red when the loading is negative. One beam failed by bond splitting (Level 3) and the others failed by shear (Level 1 and Level 2).

For specimen level 1 with 0.20mm as induced crack width, flexural and flexural-shear cracks occurred when drift angle reaches 1/400 rad. At 1/200 rad, bond splitting cracks and shear cracks occurred near the main bar of the first layer. Finally, cracks expanded and led to shear failure.

For the specimen Level 2 with 0.55mm as induced crack width, similarly to Level 1, flexural and flexural-shear cracks occurred when drift angle reaches 1/400 rad. At 1/200 rad, shear cracks took place and drastically widened just before 1/100 rad. At 1/50 rad, bond splitting cracks also developed around the rebar of the second layer. Finally, the spread of these cracks led to a complex failure mode dominated by shear.

For specimen Level 3 with 1.10mm as induced crack width, flexural and flexural-shear cracks occurred when drift angle reaches 1/400 rad. At 1/100 rad, bond splitting cracks occurred near the main bar of the first layer. This was followed by bond splitting cracks around the rebar of the second layer at 1/50 rad. Finally, the specimen failed by bond splitting.

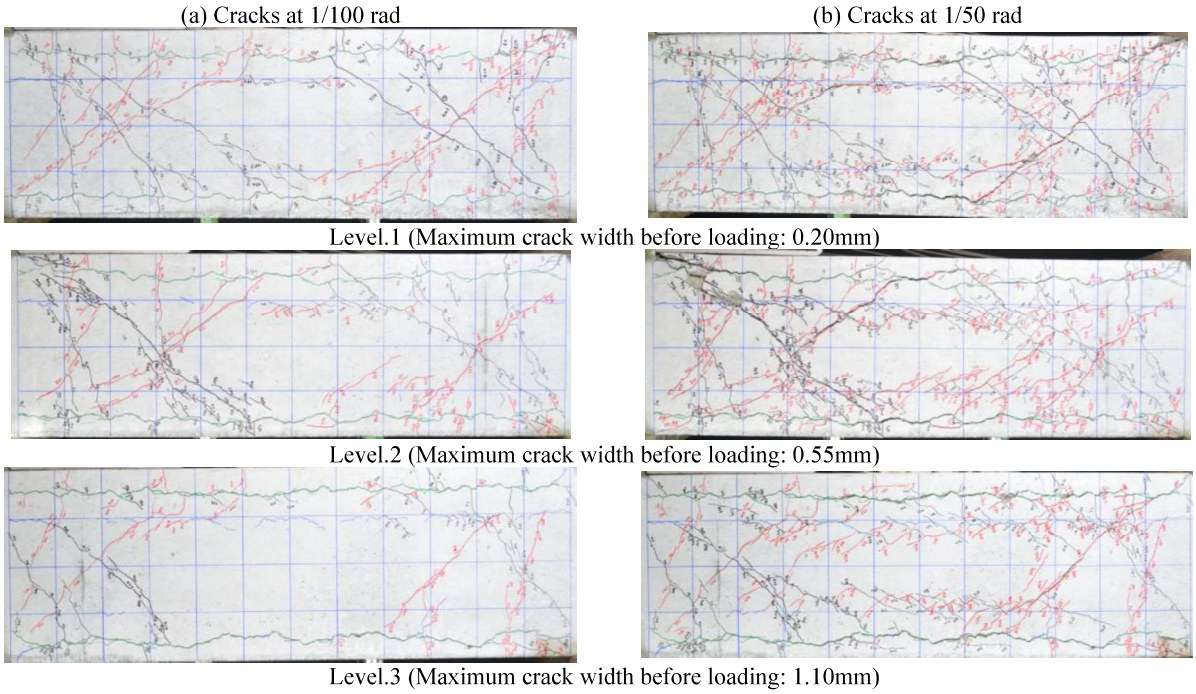

Fig.6 – Crack patterns

3.3 Shear responses of the test specimens

Shear force-drift angle hysteresis curves for each specimen are shown in Fig. 7. It can be observed that the curves of every specimen are relatively round and smooth, which shows an inverted S-shape. Moreover, after the maximum capacity, the decrease of the force tends to be severe.

For the level 1 specimen (induced crack width 0.2mm), at 1/50 rad as drift angle, the maximum positive shear force was 172 kN. However, the maximum negative shear force was -170kN at 1/100 rad. Compared to Level 1, Level 2 specimen (induced crack width 0.55mm) displays a small decrease (10%) of its maximum shear force, showing 160kN at 1/100rad and -146kN at 1/50 rad. Interestingly, the maximum shear force was observed to increase for the Level 3 specimen (induced crack width 1.10mm) when compared to Level 1 and

Level 2. Its maximum shear force was 180kN and -174kN at 1/50rad. These results are likely to be related to the deterioration of bond deterioration due to the induced crack.

Table 7 compares the maximum capacity and drift angle of tested beams, also the average of their positive and negative values is expressed. No evidence was found for degradation relations between residual shear capacity and induced crack width. This discrepancy could be attributed to the different degradation levels of the bond which is essential to the mechanism of shear resistance in RC beams. Level 3 specimen which is supposed to have the worst bond damage shows a higher shear capacity. This finding is consistent with that of Ikeda and Uji [9] who experimentally demonstrated that the shear capacity of RC beams is improved when the bond between tension rebars and concrete is destroyed. The observed increase in shear could be attributed to the arch mechanism, which is forced to form, or diagonal shear crack formation is considerably delayed. A clear benefit of induced crack width in the deterioration of shear capacity could be identified in this study. To better evaluate the shear capacity on damaged RC beams, a natural progression of this work is to analyze the effect of bond degradation on shear capacity.

Furthermore, it can be observed that the drift angle at the maximum shear force increases as the induced crack width becomes wider. This may be caused by the reduction of the stiffness when the rebar slippage is increased by bond deterioration due to induced crack.

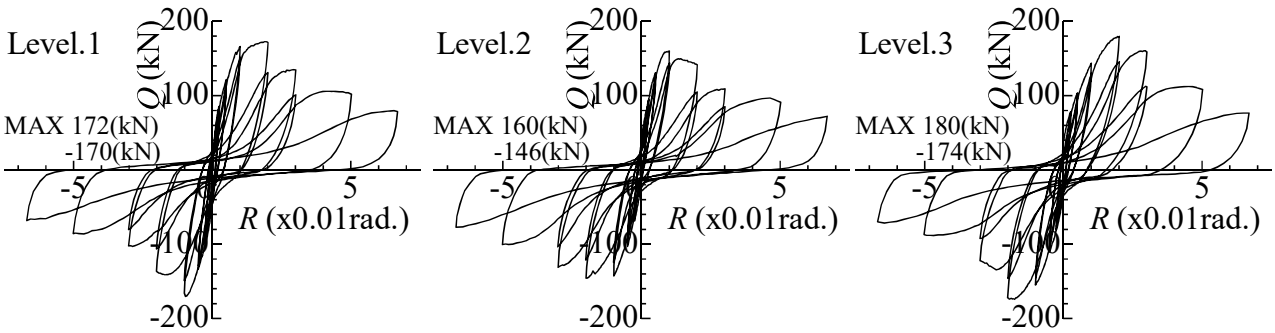

Fig.7 – Hysteresis curve

Table 7 – Test results

Specimen ID	Max. capacity (kN)		Drift angle (x0.01rad)		Ave. capacity (kN)	Ave. angle (x0.01rad)
Level.1	-170	+172	-0.91	+1.94	171	1.43
Level.2	-146	+160	-1.94	+1.01	153	1.48
Level.3	-174	+180	-1.92	+2.01	177	1.97

3.4 Comparison of skeleton curve

A skeleton curve is the envelope of all cycle loading during the loading experiment, which can reflect the seismic performance indicators of the specimen such as shear capacity, deformation, and ductility. The comparison of skeleton curves of tested beams is shown in Fig.8. Compared with Level 1 and Level 2, Level 3 shows a lower stiffness when the drift angle reaches 1/100rad. This seems to be linked with the deterioration level on the bond due to induced crack. From 1/100 rad to 1/33 rad, a higher shear capacity is observed for Level 3 specimen, however, Level 1and Level 2 show the higher shear capacity on the positive and negative side, respectively. It seems possible that the difference in the width of the induced cracks following the casting direction (as described in section 3.1) is also reflected in the cyclic behavior of the beams.

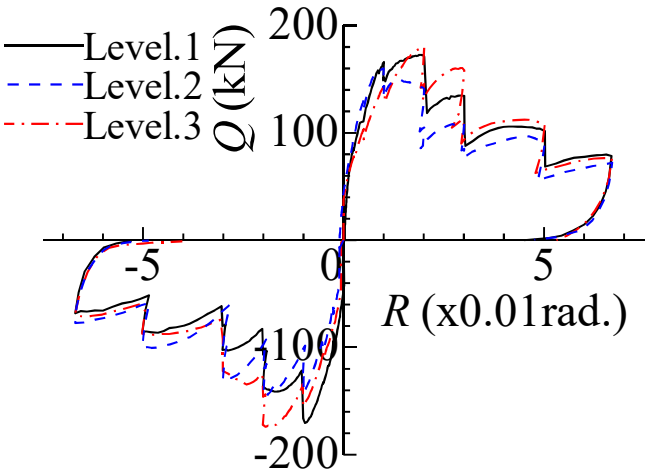

Fig.8 – Skeleton curve

3.5 Energy dissipation

The energy dissipation capacity is an important indicator to evaluate the seismic behavior of specimens, which can be determined by the enclosed area of the hysteresis curve. It is noteworthy that the structure can consume or absorb most seismic energy if it has better energy dissipation capacity under earthquake loading. Here the absorbed energy quantity for every specimen is normalized by the one obtained from Level 1. The comparison of this ratio is shown in Fig.9. As observed, the energy dissipation of Level 1 specimen is higher than those of level one. This difference can be explained in part by the decrease of shear capacity of level 2 specimen when compared to level 1. When compared to Level 1, the energy dissipation of Level 3 shows two trends. First, until 1/50 rad, the energy in Level 3 is smaller due to the degradation of stiffness caused by induced cracks. Then, after 1/50 rad with a small decrease of shear capacity, the Level 3 specimen displays bigger energy dissipation.

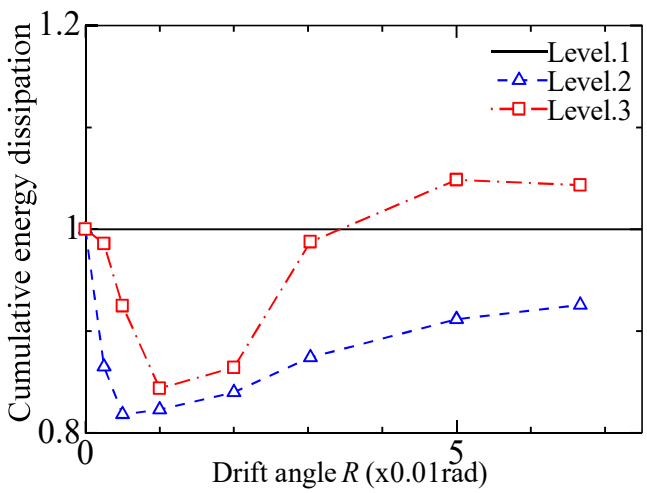

Fig.9 – Energy dissipation

4. Conclusion

Three RC beam specimens with different damage levels (induced crack width) were tested under antisymmetrical loading. Moreover, the relationship between the seismic behavior, such as shear capacity, stiffness, as well as energy dissipation, and induced crack width is described. The following conclusions can be drawn from this study.

The specimen with larger induced crack width (Level 3) failed by bond degradation along the induced cracks. However, comparative analysis of the results showed that the correlation between maximum shear capacity of specimens and induced crack width was not clear enough. Therefore, the degradation of loading capacity due to induced crack cannot be merely evaluated with the crack width parameter.

The significant modifications of service behavior were observed, due to the bond degradations, namely: loss of initial stiffness and reduction of energy dissipation. Moreover, when the bond is destroyed by to induced crack (case of Level 3), the shear capacity of the beam is improved. To better evaluate the shear on damaged RC beams, a natural progression of this work is to analyze the effect of bond degradation on shear capacity.

5. References

[1] Funaki, H., Yamakawa, T., Nakada, K. (2011): Experimental Studies on Durability and Seismic Performance of Real-Scaled RC Columns Exposed at A Coastal Area in Okinawa. *Journal of Structural and Construction Engineering, Architectural Institute of Japan*, Vol.76, No.666, 1479-1488.

[2] Maekawa K, Pimanmas A. and Okamura H (2003): *Nonlinear Mechanics of Reinforced Concrete*. Spon Press.

[3] Satoh Y. (2003): Shear Behavior of RC Member with Corroded Shear and Longitudinal Reinforcing Steels. *Proceedings of the Japanese Concrete Institute*, **25**, (1), 821-826.

[4] Murai R, Oyado M, Yasojima A, Kanakubo T (2015): Compression Failure of RC Beams Deteriorated by Corrosion, *11th Canadian Conference on Earthquake Engineering Facing Seismic Risk*, Paper ID 94182.

[5] Syll, A.S., Kawamura, Y., Kanakubo, T. (2018): Simulation of Concrete Cracks due to Bar Corrosion by Aluminum Pipe Filled with An Expansion Agent, *Summaries of Technical Papers of Annual Meeting, Architectural Institute of Japan*, Structure IV, 55-56

[6] Aburano T, Syll A S, Kanakubo T (2020): Structural Performance of RC Beams with Induced Corrosion Cracks by Aluminum Pipe Filled with an Expansion Agent, *Proceedings of the 17th World Conference on Earthquake Engineering*, Sendai, JAPAN.

[7] Architectural Institute of Japan (2010): *AIJ Standard for Structural Calculation of Reinforced Concrete Structures Based on Allowable Stress Concept*. 611-612.

[8] Architectural Institute of Japan (1990): *Design Guidelines for Earthquake Resistant Reinforced Concrete Buildings Based on Ultimate Strength Concept*. 114-127.

[9] Ikeda S, Uji K (1980): Studies on the Effect of Bond on the Shear Behavior of Reinforced Concrete Beams. *Journal. of Japan Society of Civil Engineer*, 293, 101-109.

